Journal of Fluids and Structures 18 (2003) 43–61

JOURNAL OF FLUIDS AND STRUCTURES

www.elsevier.nl/locate/jnlabr/yjfls

Aeroelastic instability of aircraft wings modelled as anisotropic composite thin-walled beams in incompressible flow

Z. Qin, L. Librescu*

Department of Engineering Science and Mechanics, Virginia Polytechnic Institute, and State University, Mail Cose (0219) Blacksburg, VA 24061-0219, USA

Received 17 April 2001; accepted 9 June 2003

Abstract

An encompassing aeroelastic model developed toward investigating the influence of directionality property of advanced composite materials and non-classical effects such as transverse shear and warping restraint on the aeroelastic instability of composite aircraft wings is presented. Within the model developed herein, both divergence and flutter instabilities are simultaneously addressed. The aircraft wing is modelled as an anisotropic composite thin-walled beam featuring circumferentially asymmetric stiffness lay-up that generates, for the problem at hand, elastic coupling among plunging, pitching and transverse shear motions. The unsteady incompressible aerodynamics used here is based on the concept of indicial functions. Issues related to aeroelastic instability are discussed, the influence of warping restraint and transverse shear on the critical speed are evaluated, and pertinent conclusions are outlined.

1. Introduction

With the stringent demands of increased performance and larger structural flexibility featured by the new generation of aerovehicles, issues involving aeroelastic behavior are among the most crucial factors toward their reliable design (Weisshaar, 1980). Due to their high structural efficiency and vast potential advantages, thin-walled structures made of anisotropic composite materials are likely to be widely used in advanced aircraft design. This was evidenced by the successful design of Gruman X-29 swept-forward wing experimental aircraft and the interest in high-altitude-long-endurance (HALE) uninhabited aerial vehicles (UAVs) (Patil and Hodges, 2000). However, in contrast to metallic structures, the composite ones exhibit significant non-classical effects such as transverse shear, warping restraint and shear stiffness variation (see, e.g., Librescu and Song, 1992; Jung et al., 1999; Song, 1990; Rehfield et al., 1990; Smith and Chopra, 1991; Librescu and Song, 1991; Song and Librescu, 1993; Na, 1997; Kim and White, 1997). Toward a reliable aeroelastic design of flight vehicles, these effects need to be assessed even in the pre-design process. In fact, within the context of solid beam or plate-beam models, the implications of transverse shear and warping restraint effects on the static divergence and flutter have been evaluated by Gern and Librescu (1998, 2000), Karpouzion and Librescu (1996), Librescu and Khdeir (1988), Librescu et al. (1996), Librescu and Simovich (1988) and Librescu and Thangjitham (1991); within the context of thin-walled beam models, Librescu and Song (1992), Song (1990), Librescu and Song (1991), Song and Librescu (1993) and Librescu et al. (1996) have investigated these effects on static divergence and free vibration; whereas within the context of a refined plate-beam model, Hwu and Tsai (2002) have investigated these effects on static divergence. As revealed in these works, non-classical effects play a complex role, and in some cases yield lower aeroelastic stability boundaries as compared with the predictions based on the classical structural model that

*Corresponding author. Tel.: +1-540-231-5916; fax: +1-540-231-4574.
E-mail address: librescu@vt.edu (L. Librescu).

0889-9746/$ - see front matter
doi:10.1016/S0889-9746(03)00082-3

Nomenclature

a_{ij}	1-D stiffness coefficients
$a(s)$	geometric quantity, related to the secondary warping (see Fig. 2)
AR	wing aspect ratio, L/b
$2b, 2d$	width and depth of the beam cross-section, respectively
b_1	inertia coefficient (see Appendix A)
$C_{L\phi}$	local lift curve slope
F_w	primary warping function (see Eq. (3))
FW + TS	free warping model, transverse shear incorporated
G_{sy}	effective membrane shear stiffness
$h_{(k)}, h$	thickness of the kth layer and of the beam wall, respectively
j	$\sqrt{-1}$
K_{ij}	reduced stiffness coefficients
L	wing semi-span
L_{ae}, T_{ae}	unsteady aerodynamic loads
m	number of truncated modes used for the calculation
n	number of aerodynamic lag terms used in the approximation of Wagner's function
N	number of polynomials used in the shape functions
U_∞	streamwise free stream speed
U_n	chordwise free stream speed, $U_\infty \cos\Lambda$
$V_{\rm cr}$	the most critical flight speed
V_F	streamwise flutter speed
w_0, ϕ	deflection, rotation about the reference axis, respectively
$\hat{w}_0, \hat{\phi}, \hat{\theta}_x$	nondimensionalized counterpart of w_0, ϕ, θ_x, respectively
WR + TS	warping restraint model, transverse shear incorporated
WR + NTR	warping restrain model, transverse shear discarded
$\mathbf{X}^{\rm T}$	transpose of the matrix or vector $\mathbf{X}$
$\mathbf{X}_{m\times n}$	$\mathbf{X}$ is a $m \times n$ matrix
γ	damping ratio
θ_x	rotation of the cross-section about the x-axis
$[\pm\theta_{n_1}/\pm\theta_{n_2}]_s$	symmetric stacking sequence
Λ	geometric sweep angle (see Fig. 1)
ρ_∞	mass density of the free stream
τ	nondimensional time variable, $U_n t/b$
ϕ_W	Wagner's function
$\hat{\mathbf{\Psi}}_w, \hat{\mathbf{\Psi}}_\phi, \hat{\mathbf{\Psi}}_x$	admissible shape functions vectors with dimension $N \times 1$
$\omega_{\rm hr}$	reference frequency, $\sqrt{a_{33}/(b_1 L^4)}\vert_{\theta=\pi/2}$
$\oint_C, \int_0^L$	integrals along the cross-section and the span, respectively
$\int_{-b}^{b}$	airfoil integral
$(\dot{(\cdot)}, \ddot{(\cdot)})$	$(\partial(\cdot)/\partial t, \partial^2(\cdot)/\partial^2 t)$
$\dot{(\cdot)}$	$\partial(\cdot)/\partial\tau$
$((\cdot)', (\cdot)'')$	$(\partial(\cdot)/\partial y, \partial^2(\cdot)/\partial y^2)$
$((\cdot)''', (\cdot)^{(\rm IV)})$	$(\partial^3(\cdot)/\partial y^3, \partial^4(\cdot)/\partial y^4)$
$(\dot{(\cdot)}', \dot{(\cdot)}'')$	$(\partial\dot{(\cdot)}/\partial\eta, \partial^2\dot{(\cdot)}/\partial\eta^2)$

discards transverse shear effect. Consequently, a better understanding of these effects constitutes a vital requirement toward a more reliable design of such types of structure. Since the aircraft design is primarily based on the principle of thin-walled beams (see, e.g., Bruhn, 1973), it is desirable to investigate the aeroelastic instability directly within the frame of thin-walled beam models. As far as the authors of this paper are aware, there are only a few papers in the open literature where the concept of thin-walled beams was used to study the aeroelastic instabilities. Within this study, a

refined thin-walled beam model primarily developed by Song (1990), Librescu and Song (1991), Song and Librescu (1993), Na (1997) and Bhaskar and Librescu (1995) is adopted and, based on it, the non-classical effects such as transverse shear and warping restraint on free vibration, divergence and flutter instabilities are investigated. As to the research work accomplished during the last two decades on the modelling of composite thin-walled beams, see recent review papers by Jung et al. (1999), Volovoi et al. (1999) and the references therein. In order to be reasonably self-contained, the basic ingredients related to this refined thin-walled beam model will be presented in the next section.

2. Formulation of the governing system

2.1. Structural model

Toward the study of aeroelastic instability of advanced aircraft wings, the concept of single-cell, closed cross-section, fiber-reinforced composite thin-walled beams is used. Due to their importance as revealed by Librescu and Song (1992), Jung et al. (1999), Song (1990), Karpouzion and Librescu (1996), Gern and Librescu (1998), Librescu et al. (1996), Gern and Librescu (2000), Librescu and Simovich (1988), Librescu and Khdeir (1988) and Librescu and Thangjitham (1991), a number of non-classical effects have to be considered, which include transverse shear, warping restraint (see, e.g., Jung et al., 1999; Song, 1990; Rehfield et al., 1990; Smith and Chopra, 1991; Kim and White, 1997), and 3-D strain effects (see, e.g., Smith and Chopra, 1991; Kim and White, 1997; Bhaskar and Librescu, 1995). It is noted that in the earlier formulation of the beam theory developed by Song (1990), Librescu and Song (1991), Song and Librescu (1993), the variation of contour-wise shear stiffness was not included. Later on, the theory was extended to account for these effects by Bhaskar and Librescu (1995). For the geometric configuration and the chosen coordinate system that is usually adopted in the analysis of aircraft wings, see Figs. 1 and 2. Based on the basic assumptions adopted by Song (1990), Librescu and Song (1991), Song and Librescu (1993) and Bhaskar and Librescu (1995), the following representation of the 3-D displacement quantities is postulated:

$$u(x,y,z,t) = u_0(y,t) + z\phi(y,t), \tag{1a}$$

$$v(x,y,z,t) = v_0(y,t) + \left[x(s) - n\frac{dz}{ds}\right]\theta_z(y,t) + \left[z(s) + n\frac{dx}{ds}\right]\theta_x(y,t) - [F_w(s) + na(s)]\phi'(y,t), \tag{1b}$$

$$w(x,y,z,t) = w_0(y,t) - x\phi(y,t), \tag{1c}$$

where

$$\theta_x(y,t) = \gamma_{yz}(y,t) - w_0'(y,t), \tag{2a}$$

$$\theta_z(y,t) = \gamma_{xy}(y,t) - u_0'(y,t), \tag{2b}$$

$$a(s) = -\left(z\frac{dz}{ds} + x\frac{dx}{ds}\right). \tag{2c}$$

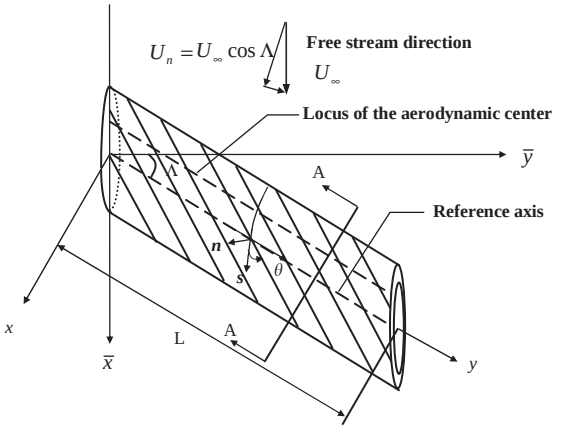

Fig. 1. Geometry of an aircraft wing modelled as thin-walled beam.

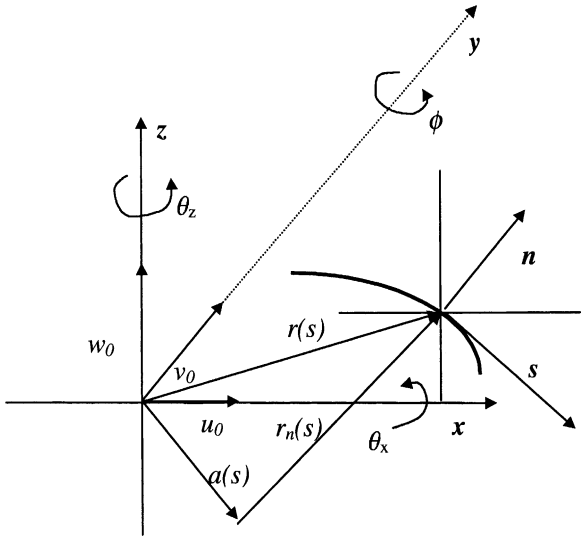

Fig. 2. Displacement field for the beam model.

In Eqs. (1) and (2), $\theta_x(y,t)$, $\theta_z(y,t)$ and $\phi(y,t)$ denote rotations of the cross-section about the axes x,z and the twist about the y-axis, respectively, $\gamma_{yz}(y,t)$ and $\gamma_{xy}(y,t)$ denote the transverse shear strains, while $a(s)$ is related to the secondary warping.

The primary warping function is expressed as

$$F_w(s) = \int_0^s [r_n(s) - \wp(s)]\,\mathrm{d}s, \tag{3}$$

where the torsional function $\wp(s)$ and the quantity $r_n(s)$ are given by

$$\wp(s) = \frac{\oint_C r_n(\bar{s})\,\mathrm{d}\bar{s}}{h(s)G_{sy}(s)\oint_C [h(\bar{s})G_{sy}(\bar{s})]^{-1}\,\mathrm{d}\bar{s}}, \quad r_n(s) = z\frac{\mathrm{d}x}{\mathrm{d}s} - x\frac{\mathrm{d}z}{\mathrm{d}s}. \tag{4}$$

In Eq. (4), G_{sy} is the effective membrane shear stiffness, which is defined as

$$G_{sy}(s) = \frac{N_{sy}}{h(s)\gamma^0_{sy}(s)}. \tag{5}$$

It is noted that G_{sy} accounts for the nonuniform shear stiffness along the contour. For the thin-walled beam theory considered herein, the six kinematic variables, i.e., $u_0(y,t)$, $v_0(y,t)$, $w_0(y,t)$, $\theta_x(y,t)$, $\theta_z(y,t)$, $\phi(y,t)$, that represent 1-D displacement measures, constitute the basic unknowns of the problem. When the transverse shear effect is discarded, Eqs. (2a) and (2b) reduce to $\theta_x = -w_0'$ and $\theta_z = -u_0'$. As a result, the basic unknown quantities are reduced to four. Such a case corresponds to the unshearable, Bernoulli–Euler beam model.

The strains that contribute to the total potential energy are as follows:

Spanwise strain:

$$\varepsilon_{yy}(n,s,y,t) = \varepsilon^0_{yy}(s,y,t) + n\varepsilon^1_{yy}(s,y,t), \tag{6a}$$

where

$$\varepsilon^0_{yy}(s,y,t) = v_0'(y,t) + \theta_z'(y,t)x(y,t) - \phi''(y,t)F_w(s), \tag{6b}$$

$$\varepsilon^1_{yy}(s,y,t) = -\theta_z'\frac{\mathrm{d}z}{\mathrm{d}s} + \theta_x'(y,t)\frac{\mathrm{d}x}{\mathrm{d}s} - a(s)\phi''(y,t); \tag{6c}$$

2-*D tangential shear strain*:

$$\gamma_{sy}(s,y,t) = \gamma^0_{sy}(s,y,t) + \wp(s)\phi'(y,t), \tag{7a}$$

where

$$\gamma_{sy}^0(s,y,t) = \gamma_{xy}\frac{\mathrm{d}x}{\mathrm{d}s} + \gamma_{yz}\frac{\mathrm{d}z}{\mathrm{d}s} = (u_0' + \theta_z)\frac{\mathrm{d}x}{\mathrm{d}s} + (w_0' + \theta_x)\frac{\mathrm{d}z}{\mathrm{d}s}; \tag{7b}$$

2-*D transverse shear strain*:

$$\gamma_{ny}(s,y,t) = -\gamma_{xy}\frac{\mathrm{d}z}{\mathrm{d}s} + \gamma_{yz}\frac{\mathrm{d}x}{\mathrm{d}s} = -(u_0' + \theta_z)\frac{\mathrm{d}z}{\mathrm{d}s} + (w_0' + \theta_x)\frac{\mathrm{d}x}{\mathrm{d}s}. \tag{8}$$

In Eqs. (6) and (7), ε_{yy}^0, γ_{sy}^0 are the normal and shear strain components on the mid-surface of the beam.

The stress resultants and stress couples can be reduced to the following expressions:

$$\begin{Bmatrix} N_{yy} \\ N_{sy} \\ L_{yy} \\ L_{sy} \end{Bmatrix} = \begin{bmatrix} K_{11} & K_{12} & K_{13} & K_{14} \\ K_{21} & K_{22} & K_{23} & K_{24} \\ K_{41} & K_{42} & K_{43} & K_{44} \\ K_{51} & K_{52} & K_{53} & K_{54} \end{bmatrix} \begin{Bmatrix} \varepsilon_{yy}^0 \\ \gamma_{sy}^0 \\ \phi' \\ \varepsilon_{yy}^1 \end{Bmatrix}, \tag{9a}$$

$$N_{ny} = [A_{44} - A_{45}^2/A_{55}]\gamma_{ny}, \tag{9b}$$

in which the reduced stiffness coefficients K_{ij} are defined by Qin and Librescu (2002).

2.2. Unsteady aerodynamic loads for arbitrary small motion in incompressible flow

Based on strip theory and 2-D incompressible unsteady aerodynamics, the unsteady aerodynamic lift and aerodynamic twist moment about the reference axis (in the present paper, the mid-chord locus is adopted as the reference axis) can be expressed as (see Fig. 3):

$$L_{ae}(y,t) = \rho_\infty U_n \Gamma_0(y,t) - \rho_\infty \frac{\mathrm{d}}{\mathrm{d}t}\int_{-b}^{b} \gamma_0(x,y,t)x\,\mathrm{d}x + \rho_\infty U_n \int_{-b}^{\infty} \frac{\gamma_w(x,y,t)}{\sqrt{x^2-b^2}}\,\mathrm{d}x, \tag{10a}$$

$$T_{ae}(y,t) = -\rho_\infty U_n \int_{-b}^{b} \gamma_0(x,y,t)x\,\mathrm{d}x + \frac{1}{2}\rho_\infty \frac{\mathrm{d}}{\mathrm{d}t}\int_{-b}^{b} \gamma_0(x,y,t)\left(x^2 - \frac{1}{2}b^2\right)\mathrm{d}x + \frac{1}{2}\rho_\infty U_n b^2 \int_{-b}^{\infty} \frac{\gamma_w(x,y,t)}{\sqrt{x^2-b^2}}\,\mathrm{d}x, \tag{10b}$$

where U_n is the free-stream speed normal to the leading edge, $\gamma_0(x,y,t)$ is the quasi-steady distributed bound vortex intensity (on the wing), $\gamma_w(x,y,t)$ is the vortex intensity in the wake, and $\Gamma_0(y,t)$ is the quasi-steady circulation. From aerodynamic potential theory, $\gamma_0(x,y,t)$ and $\gamma_w(x,y,t)$ can be uniquely determined by the boundary (no-penetration) condition and the Kutta condition (see, e.g., Katz and Plotkin, 1991, p. 428).

Expressed in the body-fixed frame (Bisplinghoff et al., 1996, Katz and Plotkin, 1991) (see Fig. 3), the vertical displacement of the wing cross-section can be expressed as

$$z_a(x,y,t) = w_0(y,t) - \phi(y,t)x, \tag{11}$$

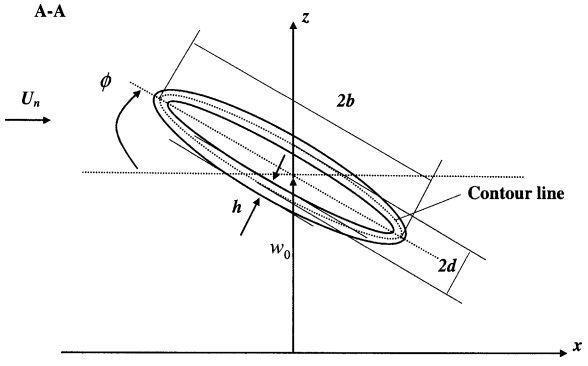

Fig. 3. Geometry of the normal cross-section.

where $w_0(y,t)$ denotes the plunging displacement and $\phi(y,t)$ being the twist about the reference axis. For the analysis of static divergence and flutter instability, it is enough to consider only the unsteady aerodynamic loads which are related to elastic deformation of the wing. They are:

$$L_{ae}(y,t) = -\pi\rho_\infty b^2 \dot{w}_{0.5c}(y,t) - 2\pi\rho_\infty U_n b\left\{ w_{0.75c}(y,0)\phi_W\left(\frac{U_n t}{b}\right) + \int_0^t \frac{\mathrm{d}w_{0.75c}(t_0)}{\mathrm{d}t_0}\,\phi_W\left[\frac{U_n}{b}(t-t_0)\right]\mathrm{d}t_0\right\}, \tag{12a}$$

$$T_{ae}(y,t) = -\pi\rho_\infty b^3\left(\frac{1}{2}U_n\dot{\phi} + \frac{1}{8}b\ddot{\phi}\right) - \pi\rho_\infty U_n b^2\left\{ w_{0.75c}(y,0)\phi_W\left(\frac{U_n t}{b}\right) + \int_0^t \frac{\mathrm{d}w_{0.75c}(t_0)}{\mathrm{d}t_0}\,\phi_W\left[\frac{U_n}{b}(t-t_0)\right]\mathrm{d}t_0\right\}, \tag{12b}$$

where ϕ_W is the indicial function for incompressible flow (also referred to as Wagner's function), defined by

$$\frac{\mathrm{d}\phi_W(\tau)}{\mathrm{d}\tau} + \phi_W(0^+)\delta(\tau) = \mathscr{L}^{-1}\left[\frac{K_1(p)}{K_0(p)+K_1(p)}\right]. \tag{12c}$$

In this equation, $\tau = U_n t/b$ is the non-dimensional time, $\mathscr{L}^{-1}$ the inverse Laplace Transform operator; p the Laplace-transform variable (i.e., the counterpart of τ), $\delta(\tau)$ the Dirac delta function, while $K_0(p)$ and $K_1(p)$ are the modified Bessel functions of the second kind (see, e.g., Sears, 1940; Meirovitch, 1997). In Eqs. (12b) and (12c), the terms in the curly brackets are associated with the *circulatory* part of the aerodynamic loads (Bisplinghoff et al., 1996; von Kármán and Sears, 1938). The quantity $K_1(p)/(K_0(p)+K_1(p)) \equiv C(p)$ is identified as the generalized Theodorsen function in the Laplace transformed space (Venkatesan and Friedmann, 1986).

In order to cast L_{ae}, T_{ae} to state space form, the quasi-polynomial approximation of the lift deficiency function is used (Bisplinghoff et al., 1996; Rodden and Stahl, 1969):

$$\phi_W(\tau) = \left[1.0 - \sum_{i=1}^{n}\alpha_i \exp(-\beta_i\tau)\right]H(\tau), \tag{13}$$

where $H(\tau)$ denotes the step function.

By denoting

$$D(y,t) \equiv \int_0^t \frac{\partial w_{0.75c}(y,t_0)}{\partial t_0}\,\phi_W\left(\frac{U_n(t-t_0)}{b}\right)\mathrm{d}t_0, \tag{13a}$$

we get

$$D(y,t) = w_{0.75c}(y,t) - \sum_{i=1}^{n}\alpha_i B_i(y,t), \tag{13b}$$

where $B_i(y,t)$ satisfies

$$\dot{B}_i + \left(\beta_i\frac{U_n}{b}\right)B_i = \dot{w}_{0.75c}(y,t). \tag{13c}$$

In the following development, we assume that the wing starts from rest.

Compared with the methods based on the transfer function realization, the above method can easily model as many as necessary aerodynamic lag terms into the finite state space form. It is noted that this method yields the same number of augmented states as those provided by the Roger's approximation method (Karpel, 1982).

The preceding results are valid for 2-D cross-section wings. For finite-span wings, the modified strip theory (Yates, 1958) that extends the 2-D aerodynamics to the 3-D case is used. As a result, in Eqs. (), (13a)–(13c), the following changes are implemented:

$$2\pi \to C_{L\phi} \equiv \frac{\mathrm{d}C_L}{\mathrm{d}\phi} = \frac{\mathrm{AR}}{AR + 2\cos\Lambda}2\pi, \quad \frac{1}{2}b \to b\left(\frac{C_{L\phi}}{2\pi} - \frac{1}{2}\right). \tag{14}$$

It is noted that only the circulatory terms in Eq. () will be modified (Yates, 1958; Rodden and Stahl, 1969). All the geometric measures are now taken in the rotated chordwise coordinate system (see Fig. 1)

$$w_{0.75c}(y,t) = \dot{w}_0 - U_n\phi + U_n\tan\Lambda\frac{\partial w_0}{\partial y} - \frac{b}{2}\left(\dot{\phi} + U_n\frac{\partial\phi}{\partial y}\tan\Lambda\right)\left(\frac{C_{L\phi}}{\pi} - 1\right), \tag{15a}$$

$$w_{0.5c}(y,t) = \dot{w}_0 - U_n\phi + U_n\tan\Lambda\frac{\partial w_0}{\partial y}, \tag{15b}$$

where $U_n = U_\infty\cos\Lambda$.

Based on these equations, the explicit expressions of unsteady aerodynamic lift and moment will be given in the following sections.

2.3. The governing system

The governing equations and the consistent boundary conditions can be systematically derived by using the principle of virtual work in dynamic case (Reddy, 1997, p. 144):

$$\int_{t_1}^{t_2} (\delta\mathscr{T} - \delta\mathscr{U} + \overline{\delta W_e})\,\mathrm{d}t = 0, \tag{16a}$$

with

$$\delta u_0 = \delta v_0 = \delta w_0 = \delta\theta_x = \delta\theta_x = \delta\phi_0 = 0 \quad \text{at } t = t_1 \text{ and } t_2, \tag{16b}$$

where $\delta\mathscr{T}$ and $\delta\mathscr{U}$ denote the virtual kinetic and strain energy, respectively, while $\overline{\delta W_e}$ denotes the virtual work due to external forces. For the problem at hand, these terms are defined as follows.

Virtual kinetic energy:

$$\delta\mathscr{T} = \int_0^L \oint_C \sum_{k=1}^{m_l} \int_{h_{(k)}} \rho_{(k)} \left[\left(\frac{\partial u}{\partial t}\right)\delta\left(\frac{\partial u}{\partial t}\right) + \left(\frac{\partial w}{\partial t}\right)\delta\left(\frac{\partial w}{\partial t}\right) + \left(\frac{\partial v}{\partial t}\right)\delta\left(\frac{\partial v}{\partial t}\right) \right] \mathrm{d}n\,\mathrm{d}s\,\mathrm{d}y; \tag{17}$$

Virtual Strain energy:

$$\delta\mathscr{V} = \int_\tau \sigma_{ij}\delta\varepsilon_{ij}\,\mathrm{d}\tau = \int_0^L \oint_C \sum_{k=1}^{m_l} \int_{h_{(k)}} [\sigma_{yy}\delta\varepsilon_{yy} + \sigma_{sy}\delta\gamma_{sy} + \sigma_{ny}\delta\gamma_{ny}]_{h_{(k)}}\,\mathrm{d}n\,\mathrm{d}s\,\mathrm{d}y; \tag{18}$$

Virtual work due to unsteady aerodynamic loads:

$$\overline{\delta W_e} = \int_0^L [L_{ae}(y,t)\delta w_0(y,t) + T_{ae}(y,t)\delta\phi(y,t)]\,\mathrm{d}y; \tag{19}$$

where L_{ae} (positive upward) is the unsteady aerodynamic lift per unit span and T_{ae} (positive nose-up) unsteady aerodynamic twist moments about the reference axis (see Eqs. (12a) and (12b)). It is recalled that for the analysis of aeroelastic instabilities, only unsteady aerodynamics need be considered.

In order to study the aeroelastic instability, an aircraft wing featuring biconvex cross-section and experiencing the bending–twist coupling is considered. To this end, the circumferentially asymmetric stiffness (CAS) lay-up (see, e.g., Rehfield et al., 1990) is adopted. As demonstrated by Librescu and Song (1991) and Song and Librescu (1993), this type of beam features the following two sets of independent elastic couplings:

(i) transversal bending/twist/vertical transverse shear (w_0, ϕ, θ_x);
(ii) extension/lateral bending/lateral transverse shear (u_0, v_0, θ_z).

Also, the unsteady aerodynamic loads and the inertia forces of the beams are completely split into the preceding two groups, hence the total equations of motion and the boundary conditions are completely decoupled. The equations of motion of the first group that are of interest for the present problem are:

$$\delta w_0 : Q_z' + L_{ae} - b_1\ddot{w}_0 = 0; \tag{20a}$$

$$\delta\phi : M_y' - B_w'' + T_{ae} - (b_4 + b_5)\ddot{\phi} + (b_{10} + b_{18})\ddot{\phi}'' = 0; \tag{20b}$$

$$\delta\theta_x : M_x' - Q_z - (b_4 + b_{14})\ddot{\theta}_x = 0. \tag{20c}$$

The boundary conditions are as follows:

$$\begin{aligned} &\text{at} \quad y = 0, \quad w_0 = 0, \quad \phi = 0, \quad \phi' = 0, \quad \theta_x = 0; \\ &\text{at} \quad y = L, \quad Q_z = 0, \quad -B_w' + M_y + (b_{10} + b_{18})\ddot{\phi}' = 0, \quad B_w = 0, \quad M_x = 0. \end{aligned} \tag{21}$$

In Eqs. (20) and (21), M_x, Q_z, B_w, M_y are the 1-D stress resultant and stress couple measures that are defined as

$$M_x(y,t)=\oint_C\left(zN_{yy}+L_{yy}\frac{\mathrm{d}x}{\mathrm{d}s}\right)\mathrm{d}s,\quad Q_z(y,t)=\oint_C\left(N_{sy}\frac{\mathrm{d}z}{\mathrm{d}s}+N_{ny}\frac{\mathrm{d}x}{\mathrm{d}s}\right)\mathrm{d}s,$$
$$B_w(y,t)=-\oint_C[F_w(s)N_{yy}+a(s)L_{yy}]\,\mathrm{d}s,\quad M_y(y,t)=\oint_C N_{sy}\wp(s)\,\mathrm{d}s. \tag{22}$$

The inertia coefficients b_1, b_4, b_5, b_{10}, b_{14}, b_{15}, b_{18} are defined in Appendix A.

For bi-convex cross-section thin-walled beams with CAS lay-up, the force–displacement relations are:

$$\begin{Bmatrix}M_x\\Q_z\\B_w\\M_y\end{Bmatrix}=\begin{bmatrix}a_{33}&0&0&a_{37}\\0&a_{55}&a_{56}&0\\0&a_{56}&a_{66}&0\\a_{37}&0&0&a_{77}\end{bmatrix}\begin{Bmatrix}\theta_x'\\(w_0'+\theta_x)\\\phi''\\\phi'\end{Bmatrix}. \tag{23}$$

For the free warping model (see, e.g., Librescu and Song, 1991; Song and Librescu, 1993; Na, 1997), the force–displacement relations are

$$\begin{Bmatrix}M_x\\Q_z\\B_w\\M_y\end{Bmatrix}=\begin{bmatrix}a_{33}&0&a_{37}\\0&a_{55}&0\\0&a_{56}&0\\a_{37}&0&a_{77}\end{bmatrix}\begin{Bmatrix}\theta_x'\\(w_0'+\theta_x)\\\phi'\end{Bmatrix}. \tag{24}$$

For the unshearable beam model (Librescu and Song, 1991; Song and Librescu, 1993; Na, 1997), the force–displacement relations are

$$\begin{Bmatrix}M_x\\Q_z\\B_w\\M_y\end{Bmatrix}=\begin{bmatrix}a_{33}&0&a_{37}\\0&a_{55}&0\\0&a_{56}&0\\a_{37}&0&a_{77}\end{bmatrix}\begin{Bmatrix}-w_0''\\\phi''\\\phi'\end{Bmatrix}. \tag{25}$$

In terms of the basic unknowns, the governing equations that include the effects of warping restraint and transverse shear are:

$$\delta w_0:a_{55}(w_0''+\theta_x')+\underline{\underline{a_{56}\phi'''}}+L_{ae}-b_1\ddot{w}_0=0; \tag{26a}$$

$$\delta\phi:a_{37}\theta_x''+a_{77}\phi''-\underline{\underline{a_{56}(w_0'''+\theta_x'')}}-\underline{\underline{a_{66}\phi^{(\mathrm{IV})}}}+T_{ae}-(b_4+b_5)\ddot{\phi}+(b_{10}+b_{18})\ddot{\phi}''=0; \tag{26b}$$

$$\delta\theta_x:a_{33}\theta_x''+a_{37}\phi''-a_{55}(w_0'+\theta_x)-\underline{\underline{a_{56}\phi''}}-\underline{(b_4+b_{14})\ddot{\theta}_x}=0. \tag{26c}$$

The associated boundary conditions are:

at $y=0$,

$$w_0=0,\quad \phi=0,\quad \underline{\underline{\phi'}}=0,\quad \theta_x=0; \tag{27a}$$

at $y=L$,

$$\begin{aligned}&\delta w_0:a_{55}(w_0'+\theta_x)+\underline{\underline{a_{56}\phi''}}=0,\\&\delta\phi:-\underline{\underline{a_{56}(w_0''+\theta_x')}}-\underline{\underline{a_{66}\phi'''}}+a_{37}\theta_x'+a_{77}\phi'=-(b_{10}+b_{18})\ddot{\phi}',\\&\underline{\underline{\delta\phi'}}:-\underline{\underline{a_{56}(w_0'+\theta_x)}}-\underline{\underline{a_{66}\phi''}}=0,\\&\delta\theta_x:a_{33}\theta_x'+a_{37}\phi'=0.\end{aligned} \tag{27b}$$

In Eqs. (26) and (27), the terms underscored by double solid lines are associated with the warping inhibition effect, whereas the term underscored by a single solid line identifies the rotatory inertia effect (see, e.g., Song, 1990; Librescu and Song, 1991; Song and Librescu, 1993).

For the unshearable beam model, the pertinent governing equations are:

$$\delta w_0 : -a_{33}w_0^{(\mathrm{IV})} + a_{37}\phi''' + L_{ae} - b_1\ddot{w}_0 + \underline{(b_4 + b_{14})\ddot{w}_0''} = 0; \tag{28a}$$

$$\delta\phi : -a_{37}w_0''' + a_{77}\phi'' - \underline{\underline{a_{66}\phi^{(\mathrm{IV})}}} + T_{ae} - (b_4 + b_5)\ddot{\phi} + (b_{10} + b_{18})\ddot{\phi}'' = 0; \tag{28b}$$

and the boundary conditions:
at $y = 0$,

$$w_0 = 0, \quad w_0' = 0, \quad \phi = 0, \quad \underline{\underline{\phi'}} = 0, \tag{29a}$$

at $y = L$,

$$\begin{aligned}
&\delta w_0 : a_{33}w_0''' - a_{37}\phi'' - (b_4 + b_{14})\ddot{w}_0' = 0,\\
&\delta w_0' : -a_{33}w_0'' + a_{37}\phi' = 0,\\
&\delta\phi : \underline{\underline{a_{66}\phi'''}} + a_{37}w_0'' - a_{77}\phi' - (b_{10} + b_{18})\ddot{\phi}' = 0,\\
&\underline{\underline{\delta\phi'}} : \underline{\underline{a_{66}\phi''}} = 0.
\end{aligned} \tag{29b}$$

It is noted that equations similar to Eqs. (28a) and (28b) obtained for solid beams have been used for static aeroelastic response (Librescu and Simovich, 1988; Librescu and Thangjitham, 1991).

The unsteady aerodynamic lift and twist moment are expressed as

$$\begin{aligned}
L_{ae}(y,t) =& -\pi\rho_\infty b^2\dot{w}_{0.5c}(y,t) - C_{L\phi}\rho_\infty U_n b\left[w_{0.75c}(y,t) - \sum_{i=1}^{n}\alpha_i B_i\right]\\
=& -\pi\rho_\infty b^2\left(\ddot{w}_0 + U_n\frac{\partial^2 w_0}{\partial y\partial t}\tan\Lambda - U_n\dot{\phi}\right)\\
&- C_{L\phi}\rho_\infty U_n b\left[\dot{w}_0 - U_n\phi + U_n\frac{\partial w_0}{\partial y}\tan\Lambda - \frac{b}{2}\left(\frac{C_{L\phi}}{\pi} - 1\right)\left(\dot{\phi} + U_n\frac{\partial\phi}{\partial y}\tan\Lambda\right) - \sum_{i=1}^{n}\alpha_i B_i\right],
\end{aligned} \tag{30a}$$

$$\begin{aligned}
T_{ae}(y,t) =& -\pi\rho_\infty b^3\left(\frac{1}{2}U_n\dot{\phi} + \frac{1}{8}b\ddot{\phi}\right) - \frac{1}{2}C_{L\phi}\rho_\infty U_n b^2\left[w_{0.75c}(y,t) - \sum_{i=1}^{n}\alpha_i B_i\right]\\
=& -\pi\rho_\infty b^3\left[\frac{1}{2}\left(\frac{C_{L\phi}}{\pi} - 1\right)\left(U_n\dot{\phi} + U_n^2\frac{\partial\phi}{\partial y}\tan\Lambda\right) + \frac{1}{8}b\left(\ddot{\phi} + U_n\frac{\partial^2\phi}{\partial y\partial t}\tan\Lambda\right)\right]\\
&- \frac{1}{2}C_{L\phi}\rho_\infty U_n b^2\left[\dot{w}_0 - U_n\phi + U_n\frac{\partial w_0}{\partial y}\tan\Lambda - \frac{b}{2}\left(\frac{C_{L\phi}}{\pi} - 1\right)\left(\dot{\phi} + U_n\frac{\partial\phi}{\partial y}\tan\Lambda\right) - \sum_{i=1}^{n}\alpha_i B_i\right].
\end{aligned} \tag{30b}$$

In Eqs. (30a) and (30b), B_i satisfies Eq. (13b).

3. Solution methodology and validation

Due to the nonconservative nature of the eigenvalue problem and the complexities arising from the anisotropy of the constituent materials and the boundary conditions, nondimensionalization and spatial semi-discretization techniques are adopted and the governing equations are cast into state-space form. The spatial semi-discretization is based on the extended Galerkin's method (EGM) (see, e.g., Librescu and Na, 1998; Palazotto and Linnemann, 1991). The conversion of the governing equations into state-space form is prompted by the fact that for a general nonconservative system, the solution requires a state-space description (Meirovitch, 1997, pp. 206–210) and the classical modal analysis based on complex eigensystem does not yield an efficient solution. It is also noted that the Laplace-transform method (LTM) can only be efficiently applied to sufficiently low-order systems. For the problem being addressed here, LTM is not the most appropriate.

3.1. State-space form of the governing equations

Introducing the following nondimensional parameters:

$$\eta \equiv y/L, \quad \tau \equiv U_n t/b, \quad AR \equiv L/b, \quad \hat{w}_0(\eta,\tau) \equiv w_0/2b,$$
$$\hat{\phi}(\eta,\tau) \equiv \phi(\eta,\tau), \quad \hat{\theta}_x(\eta,\tau) \equiv \theta_x(\eta,\tau), \quad \mathrm{d}(\cdot)/\mathrm{d}\tau = (b/U_n)\mathrm{d}(\cdot)/\mathrm{d}t, \tag{31}$$

and performing the following spatial semi-discretization:

$$\hat{w}_0(\eta,\tau) = \hat{\mathbf{\Psi}}_w^{\mathrm{T}}(\eta)\hat{\mathbf{q}}_w(\tau), \quad \hat{\phi}(\eta,\tau) = \hat{\mathbf{\Psi}}_\phi^{\mathrm{T}}(\eta)\hat{\mathbf{q}}_\phi(\tau), \quad \hat{\theta}_x(\eta,\tau) = \hat{\mathbf{\Psi}}_x^{\mathrm{T}}(\eta)\hat{\mathbf{q}}_x(\tau), \tag{32}$$

where the shape functions $\hat{\mathbf{\Psi}}_w(\eta)$, $\hat{\mathbf{\Psi}}_\phi(\eta)$, and $\hat{\mathbf{\Psi}}_x(\eta)$ are only required to fulfill the geometric boundary conditions (see Appendix B for details), we get the state-space form of the preceding aeroelastic governing equations:

$$\begin{Bmatrix} \dot{\hat{\mathbf{x}}}_s \\ \dot{\hat{\mathbf{x}}}_a \end{Bmatrix} = \begin{bmatrix} \mathbf{A}_s & \mathbf{B}_s \\ \mathbf{B}_a\mathbf{A}_s & \mathbf{A}_a + \mathbf{B}_a\mathbf{B}_s \end{bmatrix} \begin{Bmatrix} \hat{\mathbf{x}}_s \\ \hat{\mathbf{x}}_a \end{Bmatrix}, \tag{33}$$

or in a more compact form, as

$$\dot{\hat{\mathbf{X}}} = \mathbf{A}\hat{\mathbf{X}}. \tag{34}$$

In Eq. (33), $\hat{\mathbf{x}}_s$ and $\hat{\mathbf{x}}_a$ are $2m \times 1$, $nm \times 1$ vectors, which describe the motion of the wing and the unsteady aerodynamic loads on the wing, respectively. The details of the matrices and vectors in Eq. (33) are listed in Appendix B.

3.2. Static and dynamic aeroelastic instabilities

Based on Eq. (34), as described in the following, the divergence and flutter problems are solved simultaneously. Simultaneous solution of divergence and flutter is particularly convenient to aeroelastic analysis of swept composite aircraft wings. In order to address the static divergence of restrained wings, the unsteady aerodynamic terms related to the time derivatives will be discarded. Based on Eq. (34), the static aeroelastic governing equations reduce to

$$\left(k_r\bar{\mathbf{K}}_s + \frac{1}{8\mu_0}\bar{\mathbf{K}}_{ae}\right)\hat{\mathbf{q}} = \mathbf{0}. \tag{35}$$

Static divergence corresponds to the minimum flight speed that causes Eq. (35) to have nontrivial solutions.

Flutter corresponds to an eigenvalue problem. Assuming the solution in the form $\hat{\mathbf{X}} \equiv \bar{\mathbf{X}}\mathbf{e}^{\lambda\tau}$, we get

$$(\lambda\mathbf{I} - \mathbf{A})\bar{\mathbf{X}} = \mathbf{0}, \tag{36}$$

where $\lambda = \lambda_{\mathrm{Re}} + \mathrm{j}\lambda_{\mathrm{Im}}$. The flutter solution corresponds to the minimum flight speed that renders the system to transit from stable (dynamic) motion to unstable (dynamic) motion. At such a critical state, $\lambda_{\mathrm{Re}} = 0$, the imaginary part λ_{Im} corresponds to the flutter frequency. It is interesting to note that if the eigenvalue solution of Eq. (36) has a root of $\lambda_{\mathrm{Re}} > 0$, $\lambda_{\mathrm{Im}} = 0$, such an unstable root corresponds to divergence instability. Put another way, the eigenvalue solution of Eq. (36) can capture both static divergence and flutter instabilities.

3.3. Validation of the aeroelastic system model

The thin-walled beam model adopted herein has been validated by Qin and Librescu (2001, 2002). As to validate the accuracy of the aeroelastic model developed so far, several special cases are considered. The material and geometric characteristics of the wing used in this paper are listed in Table 1. As a first step, Goland's wing (Goland and Luke, 1948) is used to validate the accuracy of the flutter analysis. The results as compared in Table 2 reveal that the correlation of the present predictions with the exact results is excellent. As a second step, comparison of the flutter results by using the V–g method and the transient method is conducted, and the results are listed in Table 3. It is noted that the Theodorsen function used in the V–g method is approximated (see, e.g., Gern and Librescu, 1998; Lottati, 1985) by

$$\begin{aligned} C(k) &= F(k) + \mathrm{j}G(k) \\ &= \frac{0.021573 + 0.210400k + 0.512607k^2 + 0.500502k^3}{0.021508 + 0.251239k + 1.035378k^2 + k^3} \\ &\quad - \mathrm{j}\frac{0.001995 + 0.327214k + 0.122397k^2 + 0.000146k^3}{0.089318 + 0.934530k + 2.481481k^2 + k^3}. \end{aligned} \tag{37}$$

Table 1
Material properties and geometric characteristics of a wing featured by CAS lay-up and biconvex cross-section

	Value
Material	
E_{11}	206.8×10^9 N/m^2
$E_{22} = E_{33}$	5.17×10^9 N/m^2
$G_{13} = G_{23}$	2.55×10^9 N/m^2
G_{12}	3.10×10^9 N/m^2
$\mu_{12} = \mu_{13} = \mu_{23}$	0.25
ρ	1.528×10^3 kg/m^3
Geometric	
Width ($2b$[a])	0.259 m
Depth ($2d$[a])	0.034 m
Number of layers	7
Layer thickness	0.00123 m

[a] The length is measured on the contour line.

Table 2
Comparison of the flutter results of Goland's Wing

Method	Flutter speed (km/hr)	Error[a] (%)	Flutter frequency (Hz)	Error[a] (%)
Exact (Goland and Luke, 1948)	494.1	—	11.25	—
Present ($N = 9$), Transient method	494.5	0.08	11.04	−1.87
Present ($N = 9$), V–g method	493.2	−0.18	11.15	−0.89
Present ($N = 7$), V–g method	493.1	−0.20	11.15	−0.89
Housner and Stein (1974)	483.1	−2.23	11.27	0.18
Patil and Hodges (2000)	488.3	−1.17	11.17	−0.71
Gern and Librescu (1998) ($N = 7$)	493.6	−0.10	12.02	6.84

[a] Relative error, ([approximated] − [exact])/[exact].

Here, k is the reduced frequency, while Wagner's function is approximated by Jones' quasi-polynomial formulas (Bisplinghoff et al., 1996; Rodden and Stahl, 1969). The differences of the flutter speed and flutter frequency as predicted by these two methods are well within the approximations of the Theodorsen and Wagner's functions. However, it is interesting to note that the unstable eigenmode revealed by these two methods is quite different, as shown in Figs. 4 and 5. In Fig. 4 (via the transient method), it is shown that for the given wing, the unstable eigenmode is mode 1; while in Fig. 5 (via the V–g method), it is shown that for the same wing, the unstable eigenmode is mode 2.

4. Numerical illustrations and discussion

The aeroelastic model developed so far can be used to investigate the aeroelastic behavior of anisotropic composite aircraft wings. However, to conduct extensive parametric studies of such a type of aircraft wings is beyond the scope of the present article. In this section, the influence of anisotropy, warping restraint and transverse shear on the most critical speed (in the sense of the lowest critical speed between flutter and divergence) will be investigated. It is recalled that the divergence and flutter instabilities are simultaneously considered by the transient method.

Fig. 6 displays the most critical flight speed of an aircraft wing when the control parameter θ varies from 0° to 90°. Due to the symmetry with respect to $\theta = 90^\circ$, only the plot in the range of $[0^\circ, 90^\circ]$ is displayed. It is noted that: (i) within the range $8^\circ \leqslant \theta \leqslant 37^\circ$, divergence becomes the most critical, while (ii) within the range $45^\circ \leqslant \theta \leqslant 75^\circ$, the flutter becomes the most critical and the flutter speed is much higher than the reference speed. These two phenomena can be

Table 3
Comparison of the flutter results by the transient method and V–g method

Method	$\lambda_F = V_F/(b\omega_{\mathrm{hr}})$	$\Omega_F = \omega_F/\omega_{\mathrm{hr}}$	V_F(m/s)	ω_F(rad/s)
Transient method	53.75	7.53	235.05	87.12
V–g method	53.74	7.57	235.00	87.58

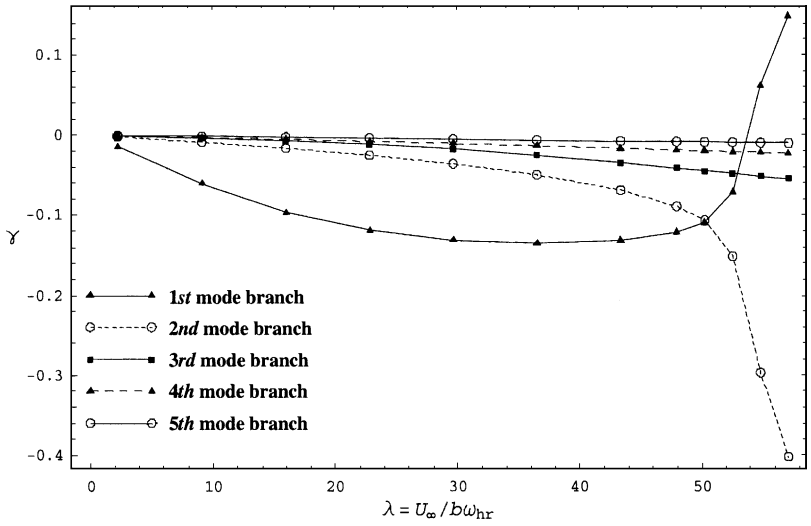

Fig. 4. Flutter analysis of a wing ($AR = 16$, $[105_6]$, $b = 0.3785$ m, $d = 0.05$ m, $\Lambda = 0^\circ$, $h = 0.01$ m) by the transient method.

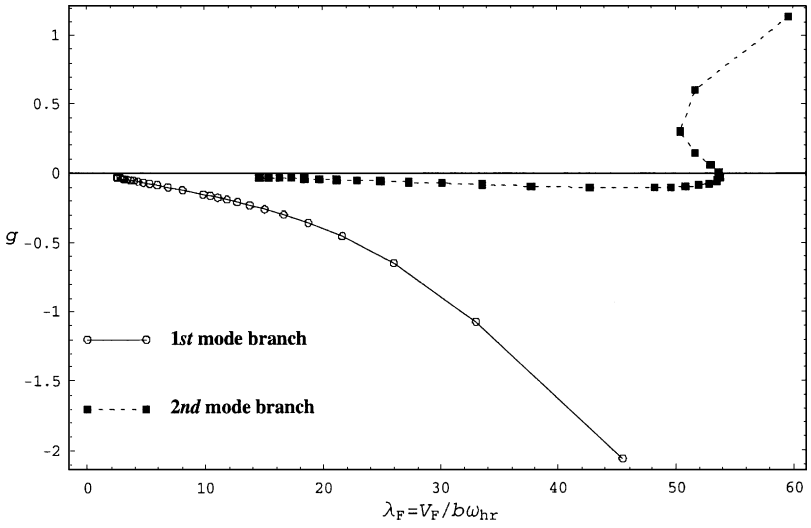

Fig. 5. Flutter analysis of a wing ($AR = 16$, $[105_6]$, $b = 0.3785$ m, $d = 0.05$ m, $\Lambda = 0^\circ$, $h = 0.01$ m) by the V–g method.

explained on the basis of the concept of washin/washout and the stiffness characteristics as displayed in Fig. 7. When θ is in the range $8^\circ \leqslant \theta \leqslant 37^\circ$, the elastic coupling a_{37} will generate nonnegligible washin, which, as is well known, leads to a low divergence speed. When θ is in the range $45^\circ \leqslant \theta \leqslant 75^\circ$, the elastic coupling a_{37} generates a washout effect, which suppresses the onset of divergence. The high flutter speed in this range of θ can be explained by the high twist (a_{77}) and bending stiffness (a_{33}). Similarly, the low flutter speed at $\theta = 0^\circ$ is due to low stiffness in twist and bending, while the low flutter speed at $\theta = 90^\circ$ is entirely due to the low twist stiffness.

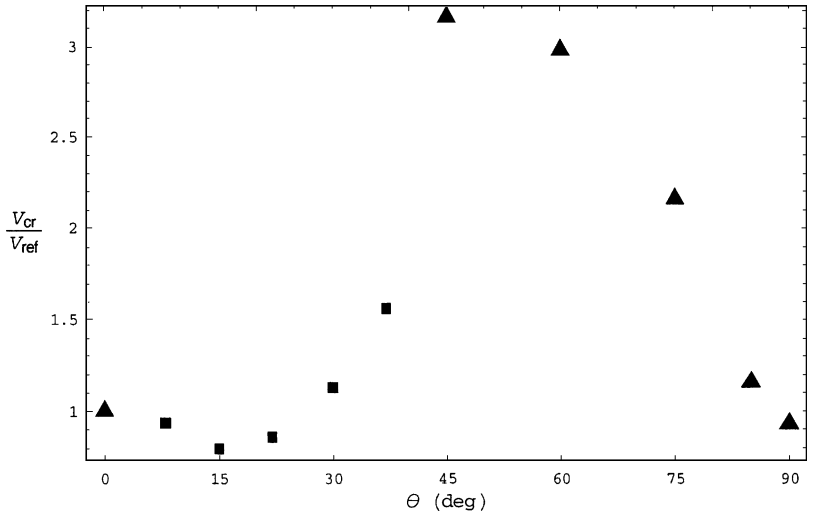

Fig. 6. Variation of the most critical flight speed of an aircraft wing versus the control parameter θ ($AR = 12$, $[2\theta/\theta/-\theta/0]_s$, $\Lambda = 0^\circ$): ▲, flutter; ▩, divergence; $V_{\text{ref}} \equiv V_{\text{cr}}|_{\theta=0^\circ}$.

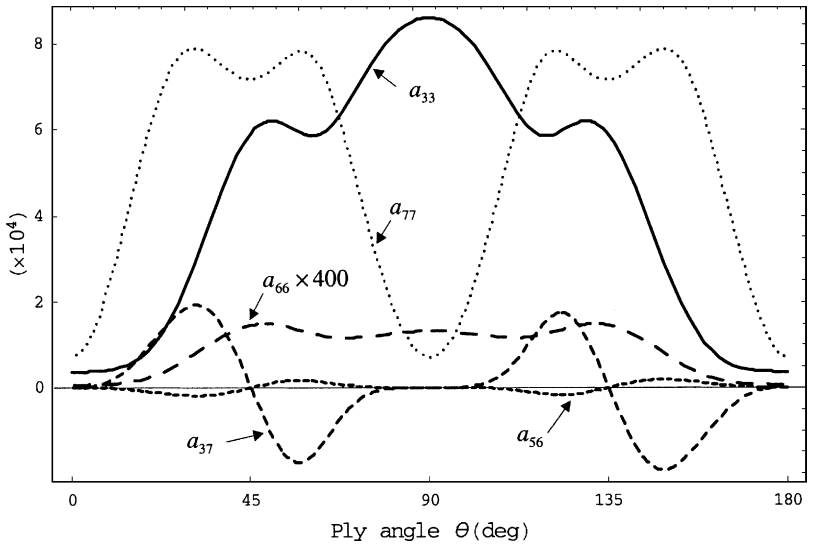

Fig. 7. Cross-sectional stiffness characteristics of an anisotropic composite aircraft wing ($[2\theta/\theta/-\theta/0]_s$).

It is well-known that swept-forward wings feature washin effect (Shirk et al., 1986), as revealed by the expression of static effective angle at the three-quarter chordwise location (measured from the leading edge):

$$\phi_{\text{eff}} \equiv -\frac{w_{0.75c}}{U_n} = \phi - \frac{\partial w_0}{\partial y}\tan\Lambda + \left(\frac{C_{L\phi}}{\phi} - 1\right)\frac{b}{2}\frac{\partial\phi}{\partial y}\tan\Lambda \tag{38}$$

which is derived from Eq. (15a) by discarding the terms associated with time derivatives. Fig. 8 displays the combined influence of the wing sweep and elastic coupling on the most critical aeroelastic instability of a swept-forward wing. It is readily seen that in this case, the washin effect induced by the sweep angle $\Lambda = -30^\circ$ exceeds the washout effect induced by the elastic coupling a_{37} when $45^\circ \leqslant \theta \leqslant 90^\circ$, and the divergence is the most critical one over the entire range $0^\circ \leqslant \theta \leqslant 90^\circ$. The maximum divergence speed occurring at $\theta = 60^\circ$ (about 3.5 times higher than the reference speed!) can be explained by the fact that, on the one hand, the washout effect induced by a_{37} reaches its maximum and, on the other hand, that the twist stiffness also reaches its maximum. It is also interesting to note that although the twist stiffness a_{77} and the elastic coupling stiffness a_{37} at $\theta = 90^\circ$ are equal to those at $\theta = 0^\circ$, the most critical speed at $\theta = 90^\circ$ is about

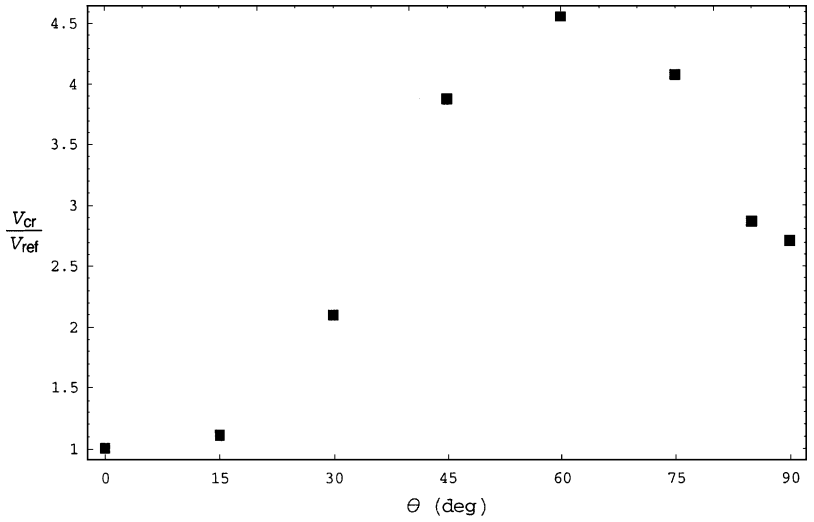

Fig. 8. Combined influence of sweep angle and elastic coupling on divergence of a swept-forward wing ($AR = 12$, $[2\theta/\theta/-\theta/0]_s$, $\Lambda = -30^\circ$), $V_{ref} \equiv V_{cr}|_{\theta=0^\circ}$.

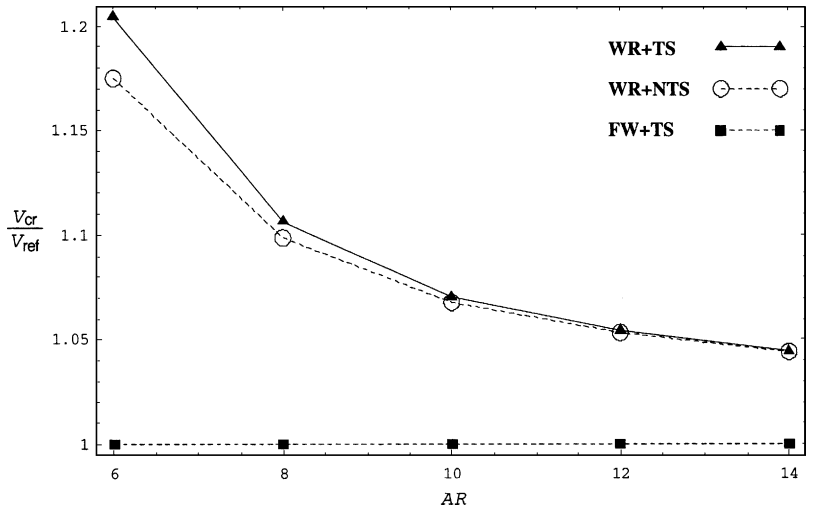

Fig. 9. Influence of warping restraint and transverse shear on flutter of an aircraft wing ($\Lambda = 0^\circ$, $[0/90_2/0]_s$), V_{ref} is defined as V_{cr}, predicted by the FW + TS model.

2.7 times its counterpart at $\theta = 0^\circ$. This, again, can be explained by the washout effect as revealed by Eq. (38): from Fig. 7, the bending stiffness a_{33} at $\theta = 90^\circ$ is much larger than that at $\theta = 0^\circ$, therefore, the washout generated in the case of $\theta = 90^\circ$ will be much less than its counterpart in the case of $\theta = 0^\circ$.

Figs. 9 and 10 display the influence of warping restraint and transverse shear on the aeroelastic instabilities. In Fig. 9, flutter is the most critical; while in Fig. 10, divergence is the most critical. In both figures, the significant influence of warping restraint on the flutter and divergence speed is revealed, that is: 20% increase of flutter speed when $AR = 6$ (see Fig. 9), and 12% increase of divergence speed when $AR = 6$ (see Fig. 10). Even for large aspect ratio wings, e.g., $AR = 14$, there is still about 5% increase of the most critical speed compared with the prediction by the free warping model. In contrast to such a significant influence of warping restraint on divergence and flutter, the transverse shear has a marginal influence on the most critical speeds in these two cases (about 3% or less difference from the prediction by discarding the transverse shear). However, it is quite remarkable to note that in Fig. 9 the discard of transverse shear yields *lower* flutter speed than otherwise, while in Fig. 10 discarding the transverse shear predicts, inadvertently, *higher*

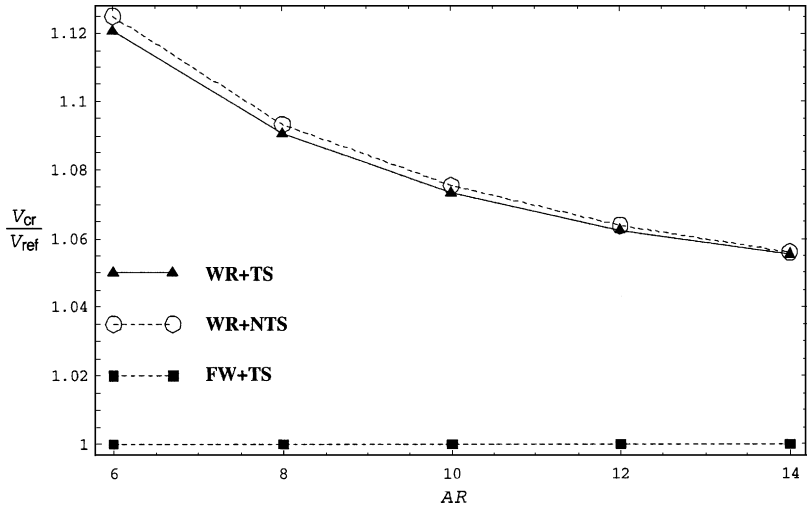

Fig. 10. Influence of warping restraint and transverse shear on divergence of an aircraft wing ($\Lambda = 0^\circ$, $[75_7]$), V_{ref} is defined as V_{cr}, predicted by the FW + TS model.

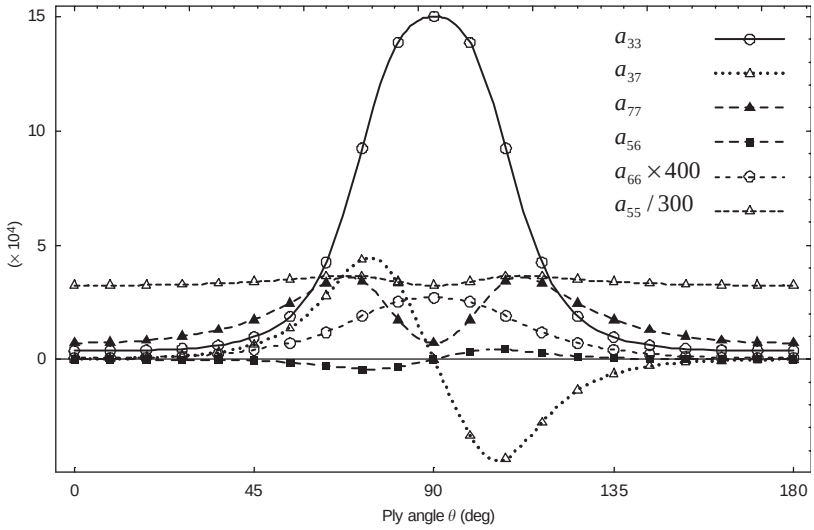

Fig. 11. Cross-sectional stiffness characteristics of an anisotropic composite aircraft wings ($[\theta_7]$).

divergence speed. For the former case, it is safe to discard the transverse shear from the point of view of design, while in the latter case, the discard of the transverse shear yields an inadvertent overestimation of the divergence instability. It is scrutinized that this higher predicted divergence speed in Fig. 10 (although the amplitude of the difference is marginal) can be explained by the characteristic of elastic coupling a_{37}, which is displayed in Fig. 11: at $\theta = 75^\circ$, a_{37} generates washin effect (i.e., increase of w_0 will induce nose-up twist ϕ, see Eq. (28)), therefore, discarding the transverse shear in such a case tends to nullify the washin effect, hence leading to higher divergence speed.

5. Conclusions

An encompassing aeroelastic model of anisotropic composite wings in the form of a thin-walled beam has been developed and validated. Due to the large number of involved parameters, extensive parametric studies are beyond the scope of the present article. Instead, only a few cases related to the influence of anisotropy, warping restraint and

transverse shear on the most critical speed have been actually investigated. The major conclusions from these studied cases are as follows.

(i) the directionality property of anisotropic composite materials plays a complex role on the aeroelastic instability; however, as revealed by the cases studied, this complex role can be explained by well established aeroelastic concepts such as washin, washout, twist/bending stiffness and coupling among them.
(ii) the warping restraint effect has a significant influence on both the flutter and divergence speeds when the aspect ratio is moderate ($6 \leqslant AR \leqslant 10$). This effect should be considered in the design process.
(iii) in the cases studied in the present article, it appears that transverse shear deformation has a marginal influence on the aeroelastic instability. However, the results show that the discard of transverse shear does not always yield conservative predictions.

Appendix A. Expression of 1-D stiffness and the inertia coefficients

The global stiffness quantities $a_{ij}(=a_{ji})$ and inertia terms b_i related to the problem are defined as

$$a_{33} = \oint_C \left[z^2 K_{11} + 2z \frac{\mathrm{d}x}{\mathrm{d}s} K_{14} + \left(\frac{\mathrm{d}x}{\mathrm{d}s}\right)^2 K_{44} \right] \mathrm{d}s, \quad a_{37} = \oint_C \left[z K_{13} + \frac{\mathrm{d}x}{\mathrm{d}s} K_{43} \right] \mathrm{d}s,$$

$$a_{55} = \oint_C \left[\left(\frac{\mathrm{d}z}{\mathrm{d}s}\right)^2 K_{22} + \left(\frac{\mathrm{d}x}{\mathrm{d}s}\right)^2 \bar{A}_{44} \right] \mathrm{d}s, \quad a_{56} = -\oint_C \left[F_w \frac{\mathrm{d}z}{\mathrm{d}s} K_{21} + a(s) \frac{\mathrm{d}z}{\mathrm{d}s} K_{24} \right] \mathrm{d}s,$$

$$a_{66} = \oint_C [F_w^2 K_{11} + 2F_w a(s) K_{14} + a(s)^2 K_{44}] \, \mathrm{d}s, \quad a_{77} = \oint_C \wp(s) K_{23} \, \mathrm{d}s,$$

where K_{ij} are the reduced stiffness coefficients and $\bar{A}_{44} = A_{44} - A_{45}^2/A_{55}$.

The inertia coefficients in Eq. (20) are defined as

$$b_1 = \oint_C m_0 \, \mathrm{d}s, \quad (b_4, b_5) = \oint_C (z^2, x^2) m_0 \, \mathrm{d}s, \quad b_{14} = \oint_C m_2 \left(\frac{\mathrm{d}x}{\mathrm{d}s}\right)^2 \mathrm{d}s,$$

$$b_{15} = \oint_C m_2 \left(\frac{\mathrm{d}z}{\mathrm{d}s}\right)^2 \mathrm{d}s \quad (b_{10}, b_{18}) = \oint_C (m_0 F_w^2(s), m_2 a^2(s)) \, \mathrm{d}s,$$

in which

$$(m_0, m_2) = \sum_{k=1}^{m_l} \int_{h_{(k)}^-}^{h_{(k)}^+} \rho_{(k)} (1, n^2) \, \mathrm{d}n.$$

Appendix B. Definition of matrices in Eq. (33)

The definitions are simply listed, as follows.

$$[\mathbf{A}] = \begin{bmatrix} \mathbf{A}_s & \mathbf{B}_s \\ \mathbf{B}_a \mathbf{A}_s & \mathbf{A}_a + \mathbf{B}_a \mathbf{B}_s \end{bmatrix}, \quad [\mathbf{A}_s]_{2m\times 2m} = \begin{bmatrix} 0_{m\times m} & \mathbf{I}_{m\times m} \\ -\bar{\mathbf{M}}_n^{-1} \bar{\mathbf{K}}_n & -\bar{\mathbf{M}}_n^{-1} \bar{\mathbf{C}}_n \end{bmatrix},$$

$$[\mathbf{B}_s]_{2m\times nm} = \begin{bmatrix} \mathbf{0}_{m\times nm} \\ \dfrac{1}{8\mu_0} \bar{\mathbf{M}}_n^{-1} [\alpha_1 \mathbf{I}_{m\times m} \cdots \alpha_n \mathbf{I}_{m\times m}]_{m\times nm} \end{bmatrix},$$

$$[\mathbf{A}_a]_{nm\times nm} = \begin{bmatrix} -\beta_1 \mathbf{I}_{m\times m} & & \\ & \ddots & \\ & & -\beta_n \mathbf{I}_{m\times m} \end{bmatrix}, \quad [\mathbf{B}_a]_{nm\times 2m} = \begin{bmatrix} \mathbf{I}_{m\times m} \\ \vdots \\ \mathbf{I}_{m\times m} \end{bmatrix}_{nm\times m} \quad [\mathbf{D}_1 \;\; \mathbf{D}_2]_{m\times 2m},$$

$$\bar{\mathbf{M}}_n = \mathbf{\Theta}^{\mathrm{T}}(\bar{\mathbf{M}}_s + \frac{1}{8\mu_0}\bar{\mathbf{M}}_{ae})\mathbf{\Theta}, \quad \bar{\mathbf{C}}_n = \frac{1}{8\mu_0}\mathbf{\Theta}^{\mathrm{T}}\bar{\mathbf{C}}_{ae}\mathbf{\Theta},$$
$$\bar{\mathbf{K}}_n = \mathbf{\Theta}^{\mathrm{T}}(k_r\bar{\mathbf{K}}_s + \frac{1}{8\mu_0}\bar{\mathbf{K}}_{ae})\mathbf{\Theta};$$

$$\mathbf{D}_1 = \frac{C_{L\phi}}{\pi}\mathbf{\Theta}_w^{\mathrm{T}}\left\{\frac{2}{AR}\tan\Lambda\int_0^1 \hat{\mathbf{\Psi}}_w\hat{\mathbf{\Psi}}_w'^{\mathrm{T}}\,\mathrm{d}\eta\mathbf{\Theta}_w - \int_0^1\left[\hat{\mathbf{\Psi}}_w\hat{\mathbf{\Psi}}_\phi^{\mathrm{T}} + \left(\frac{C_{L\phi}}{\pi}-1\right)\frac{\tan\Lambda}{2AR}\hat{\mathbf{\Psi}}_w\hat{\mathbf{\Psi}}_\phi'^{\mathrm{T}}\,\mathrm{d}\eta\mathbf{\Theta}_\phi\right]\right\}$$
$$+\frac{C_{L\phi}}{2\pi}\mathbf{\Theta}_\phi^{\mathrm{T}}\left\{\frac{1}{AR}\tan\Lambda\int_0^1 \hat{\mathbf{\Psi}}_\phi\hat{\mathbf{\Psi}}_w'^{\mathrm{T}}\,\mathrm{d}\eta\mathbf{\Theta}_w - \frac{1}{2}\int_0^1\left[\hat{\mathbf{\Psi}}_\phi\hat{\mathbf{\Psi}}_\phi^{\mathrm{T}} + \left(\frac{C_{L\phi}}{\pi}-1\right)\frac{\tan\Lambda}{2AR}\hat{\mathbf{\Psi}}_\phi\hat{\mathbf{\Psi}}_\phi'^{\mathrm{T}}\right]\mathrm{d}\eta\mathbf{\Theta}_\phi\right\},$$

$$\mathbf{D}_2 = \frac{C_{L\phi}}{\pi}\mathbf{\Theta}_w^{\mathrm{T}}\left[2\int_0^1 \hat{\mathbf{\Psi}}_w\hat{\mathbf{\Psi}}_w^{\mathrm{T}}\,\mathrm{d}\eta\mathbf{\Theta}_w - \frac{1}{2}\left(\frac{C_{L\phi}}{\pi}-1\right)\int_0^1\hat{\mathbf{\Psi}}_w\hat{\mathbf{\Psi}}_\phi^{\mathrm{T}}\,\mathrm{d}\eta\mathbf{\Theta}_\phi\right]$$
$$+\frac{C_{L\phi}}{2\pi}\mathbf{\Theta}_\phi^{\mathrm{T}}\left[\int_0^1 \hat{\mathbf{\Psi}}_\phi\hat{\mathbf{\Psi}}_w^{\mathrm{T}}\,\mathrm{d}\eta\mathbf{\Theta}_w - \frac{1}{4}\left(\frac{C_{L\phi}}{\pi}-1\right)\int_0^1\hat{\mathbf{\Psi}}_\phi\hat{\mathbf{\Psi}}_\phi^{\mathrm{T}}\,\mathrm{d}\eta\mathbf{\Theta}_\phi\right],$$

$$\bar{\mathbf{M}}_s = \int_0^1\begin{bmatrix}\hat{\mathbf{\Psi}}_w\hat{\mathbf{\Psi}}_w^{\mathrm{T}} & 0 & 0\\ 0 & \hat{I}_t\hat{\mathbf{\Psi}}_\phi\mathbf{\Psi}_\phi^{\mathrm{T}} + \hat{I}_w\hat{\mathbf{\Psi}}_\phi'\hat{\mathbf{\Psi}}_\phi'^{\mathrm{T}} & 0\\ 0 & 0 & \hat{r}^2\hat{\mathbf{\Psi}}_x\hat{\mathbf{\Psi}}_x^{\mathrm{T}}\end{bmatrix}\mathrm{d}\eta,$$

$$\bar{\mathbf{K}}_s = \int_0^1\begin{bmatrix}\frac{4}{AR^2}\hat{\mathbf{\Psi}}_w'\hat{\mathbf{\Psi}}_w'^{\mathrm{T}} & \frac{2}{AR}\mu_1 c_{14}\underline{\underline{\hat{\mathbf{\Psi}}_w'\hat{\mathbf{\Psi}}_\phi''^{\mathrm{T}}}} & \frac{2}{AR}\hat{\mathbf{\Psi}}_w'\mathbf{\Psi}_x^{\mathrm{T}}\\ & \frac{4}{AR^2}\mu_1\mu_2\underline{\underline{\hat{\mathbf{\Psi}}_\phi''\hat{\mathbf{\Psi}}_\phi''^{\mathrm{T}}}} + \mu_1 c_{12}\hat{\mathbf{\Psi}}_\phi'\hat{\mathbf{\Psi}}_\phi'^{\mathrm{T}} & \mu_1 c_{14}\underline{\underline{\hat{\mathbf{\Psi}}_\phi''\hat{\mathbf{\Psi}}_x^{\mathrm{T}}}} + \mu_1 c_{13}\hat{\mathbf{\Psi}}_\phi'\hat{\mathbf{\Psi}}_x'^{\mathrm{T}}\\ \text{symm} & & (\mu_1\hat{\mathbf{\Psi}}_x'\hat{\mathbf{\Psi}}_x'^{\mathrm{T}} + \hat{\mathbf{\Psi}}_x\hat{\mathbf{\Psi}}_x^{\mathrm{T}})\end{bmatrix}\mathrm{d}\eta,$$

$$\bar{\mathbf{M}}_{ae} = \int_0^1\begin{bmatrix}2\hat{\mathbf{\Psi}}_w\hat{\mathbf{\Psi}}_w^{\mathrm{T}} & 0 & 0\\ 0 & \frac{1}{16}\hat{\mathbf{\Psi}}_\phi\hat{\mathbf{\Psi}}_\phi^{\mathrm{T}} & 0\\ 0 & 0 & 0\end{bmatrix}\mathrm{d}\eta,$$

$$\bar{\mathbf{C}}_{ae} = \int_0^1\begin{bmatrix}\frac{2}{AR}\tan\Lambda\hat{\mathbf{\Psi}}_w\hat{\mathbf{\Psi}}_w'^{\mathrm{T}} + \frac{2C_{L\phi}}{\pi}\hat{\mathbf{\Psi}}_w\hat{\mathbf{\Psi}}_w^{\mathrm{T}} & -\left[1+\frac{C_{L\phi}}{2\pi}\left(\frac{C_{L\phi}}{\pi}-1\right)\right]\hat{\mathbf{\Psi}}_w\hat{\mathbf{\Psi}}_\phi^{\mathrm{T}} & 0\\ \frac{C_{L\phi}}{2\pi}\hat{\mathbf{\Psi}}_\phi\hat{\mathbf{\Psi}}_w^{\mathrm{T}} & \frac{1}{16\,AR}\tan\Lambda\hat{\mathbf{\Psi}}_\phi\hat{\mathbf{\Psi}}_\phi'^{\mathrm{T}} & \\ & +\frac{1}{4}\left(\frac{C_{L\phi}}{\pi}-1\right)\left(1-\frac{C_{L\phi}}{2\pi}\right)\hat{\mathbf{\Psi}}_\phi\hat{\mathbf{\Psi}}_\phi^{\mathrm{T}} & 0\\ 0 & 0 & 0\end{bmatrix}\mathrm{d}\eta,$$

$$\bar{\mathbf{K}}_{ae} = \int_0^1\begin{bmatrix}\frac{2C_{L\phi}}{\pi AR}\tan\Lambda\hat{\mathbf{\Psi}}_w\hat{\mathbf{\Psi}}_w'^{\mathrm{T}} & -\frac{C_{L\phi}}{\pi}\hat{\mathbf{\Psi}}_w\hat{\mathbf{\Psi}}_\phi^{\mathrm{T}} - \frac{C_{L\phi}}{2\pi AR}\left(\frac{C_{L\phi}}{\pi}-1\right)\tan\Lambda\hat{\mathbf{\Psi}}_w\hat{\mathbf{\Psi}}_\phi'^{\mathrm{T}} & 0\\ \frac{C_{L\phi}}{2\pi AR}\tan\Lambda\hat{\mathbf{\Psi}}_\phi\hat{\mathbf{\Psi}}_w'^{\mathrm{T}} & -\frac{C_{L\phi}}{4\pi}\hat{\mathbf{\Psi}}_\phi\hat{\mathbf{\Psi}}_\phi^{\mathrm{T}} + \left(1-\frac{C_{L\phi}}{2\pi}\right)\left(\frac{C_{L\phi}}{\pi}-1\right)\frac{\tan\Lambda}{4AR}\hat{\mathbf{\Psi}}_\phi\hat{\mathbf{\Psi}}_\phi'^{\mathrm{T}} & 0\\ 0 & 0 & 0\end{bmatrix}\mathrm{d}\eta.$$

In the above expressions, $\hat{\mathbf{\Psi}}_w(\eta)$, $\hat{\mathbf{\Psi}}_\phi(\eta)$, and $\hat{\mathbf{\Psi}}_x(\eta)$ are shape function vectors (with dimension $N\times 1$) which are required to only fulfill the geometric boundary conditions. For the model incorporating both the warping restraint and transverse shear (i.e., WR + TS model), $\hat{\mathbf{\Psi}}_w(\eta) = [\eta,\ \eta^2,\ \ldots,\eta^N]^{\mathrm{T}}$, $\hat{\mathbf{\Psi}}_\phi(\eta) = [\eta^2,\ \eta^3,\ \ldots,\eta^{N+1}]^{\mathrm{T}}$, $\hat{\mathbf{\Psi}}_x(\eta) = [\eta,\ \eta^2,\ \ldots,\eta^N]^{\mathrm{T}}$ are adopted in the article. $\mathbf{\Theta}_w$, $\mathbf{\Theta}_\phi$, $\mathbf{\Theta}_x$ are $N\times m$ eigenvectors and $\mathbf{\Theta}\equiv[\mathbf{\Theta}_w^{\mathrm{T}}\ \mathbf{\Theta}_\phi^{\mathrm{T}}\ \mathbf{\Theta}_x^{\mathrm{T}}]^{\mathrm{T}}$.

Appendix C. Nondimensional parameters

The nondimensional parameters used in the text and Appendix B are defined as

$$\mu_0 = \frac{b_1}{\pi\rho_\infty(2b)^2}, \quad \mu_1 = \frac{a_{33}}{a_{55}L^2}, \quad \mu_2 = \frac{a_{66}}{a_{33}(2b)^2}, \quad \omega_h^2 = \frac{a_{33}}{b_1L^4},$$

$$\omega_{hr} = \omega_h|_{\theta=\pi/2}, \quad \hat{r} = \sqrt{\frac{(b_4+b_{14})}{b_1L^2}}, \quad c_{12} = \frac{a_{77}}{a_{33}}, \quad c_{13} = \frac{a_{37}}{a_{33}},$$

$$c_{14} = \frac{a_{56}}{a_{33}}, \quad \hat{I}_t = \frac{(b_4+b_5)}{(2b)^2b_1}, \quad \hat{I}_w = \frac{(b_{10}+b_{18})}{L^2(2b)^2b_1}, \quad k_r = \frac{a_{55}}{4b_1U_n^2}.$$

References

Bhaskar, K., Librescu, L., 1995. A geometrically non-linear theory for laminated anisotropic thin-walled beams. International Journal of Engineering Science 33, 1331–1344.

Bisplinghoff, R.L., Ashley, H., Halfman, R.L., 1996. Aeroelasticity. Dover Publications, New York.

Bruhn, E.F., 1973. Analysis and Design of Flight Vehicle Structures. Jacobs Publishing, Indianapolis, IN.

Gern, F., Librescu, L., 1998. Static and dynamic aeroelasticity of advanced aircraft wings carrying external stores. AIAA Journal 36, 1121–1129.

Gern, F., Librescu, L., 2000. Aeroelastic tailoring of composite wings exhibiting nonclassical effects and carrying external stores. Journal of Aircraft 37, 1097–1104.

Goland, M., Luke, Y., 1948. The flutter of a uniform cantilever wing with tip weights. Journal of Applied Mechanics 15, 13–20.

Housner, J.M., Stein, M., 1974. Flutter analysis of swept-wing sunsonic aircraft with parameter studies of composite wings. Technical Report NASA TN-D-7539.

Hwu, C., Tsai, Z.S., 2002. Aeroelastic divergence of stiffened composite multicell wing structures. Journal of Aircraft 39, 242–251.

Jung, S.N., Nagaraj, V.T., Chopra, I., 1999. Assessment of composite rotor blade modeling techniques. Journal of the American Helicopter Society 44, 188–205.

Karpel, M., 1982. Design of active flutter suppression and gust alleviation using state-space aeroelastic modeling. Journal of Aircraft 19, 221–227.

Karpouzion, G., Librescu, L., 1996. Nonclassical effects on divergence and flutter of anisotropic swept aircraft wings. AIAA Journal 34, 786–794.

Katz, J., Plotkin, A., 1991. Low-Speed Aerodynamics: From Wing Theory to Panel Methods. McGraw-Hill, New York, pp. 451–457.

Kim, C., White, S.R., 1997. Thick-walled composite beam theory including 3-D elastic effects and torsional warping. International Journal of Solids and Structures 34, 4237–4259.

Librescu, L., Khdeir, A., 1988. Aeroelastic divergence of swept-forward composite wings including warping restraint effect. AIAA Journal 26, 1373–1377.

Librescu, L., Na, S.S., 1998. Dynamic response of cantilevered thin-walled beams to blast and sonic-boom loadings. Shock and Vibration 5, 23–33.

Librescu, L., Simovich, J., 1988. General formulation for the aeroelastic divergence of composite swept-forward wing structures. Journal of Aircraft 25, 364–371.

Librescu, L., Song, O., 1991. Behavior of thin-walled beams made of advanced composite materials and incorporating non-classical effects. Applied Mechanics Reviews 44 (11, Part 2), S174–S180.

Librescu, L., Song, O., 1992. On the static aeroelastic tailoring of composite aircraft swept wings modeled as thin-walled beam structures. Composites Engineering 2, 497–512.

Librescu, L., Thangjitham, S., 1991. Analytical studies on static aeroelastic behavior of forward-swept composite wing structures. Journal of Aircraft 28, 151–157.

Librescu, L., Meirovitch, L., Song, O., 1996. Refined structural modeling for enhancing vibrations and aeroelastic characteristics of composite aircraft wings. La Recherche Aérospatiale 1, 23–35.

Lottati, I., 1985. Flutter and divergence aeroelastic characteristics for composite forward swept cantilevered wing. Journal of Aircraft 22, 1001–1007.

Meirovitch, L., 1997. Principles and Techniques of Vibrations. Prentice-Hall, Upper Saddle River, NJ, pp. 189–194.

Na, S.S., 1997. Control of dynamic response of thin-walled composite beams using structural tailoring and piezoelectric actuation. Ph.D. Thesis, Virginia Polytechnic Institute and State University.

Palazotto, A.N., Linnemann, P.E., 1991. Vibration and buckling characteristics of composite cylindrical panels incorporating the effects of a higher order shear theory. International Journal of Solids and Structures 28, 341–361.

Patil, M.J., Hodges, D.H., 2000. Nonlinear aeroelastic analysis of composite aircraft in subsonic flow. Journal of Aircraft 37, 751–760.

Qin, Z., Librescu, L., 2001. Static and dynamic validations of a refined thin-walled composite beam model. AIAA Journal 39, 2422–2424.

Qin, Z., Librescu, L., 2002. On a shear-deformable theory of anisotropic thin-walled beams: Further contribution and validation. Journal of Composite Structures 56, 345–358.

Reddy, J.N., 1997. Mechanics of Laminated Composite Plates. CRC Press, Boca Raton, FL.

Rehfield, L.W., Atilgan, A.R., Hodges, D.H., 1990. Nonclassical behavior of thin-walled composite beams with closed cross sections. Journal of the American Helicopter Society 35, 42–51.

Rodden, W.P., Stahl, B., 1969. A strip method for prediction of damping in subsonic wind tunnel and flight flutter tests. Journal of Aircraft 6, 9–17.

Sears, W.R., 1940. Operational methods in the theory of airfoils in non-uniform motion. Journal of the Franklin Institute 230, 94–111.

Shirk, M.H., Hertz, T.J., Weisshaar, T.A., 1986. Aeroelastic tailoring-theory, practice, and promise. Journal of Aircraft 23, 6–18.

Smith, E.C., Chopra, I., 1991. Formulation and evaluation of an analytical model for composite box-beams. Journal of American Helicopter Society 36, 23–35.

Song, O., 1990. Modeling and response analysis of thin-walled beam structures constructed of advanced composite materials. Ph.D. Thesis, Virginia Polytechnic Institute and State University.

Song, O., Librescu, L., 1993. Free vibration of anisotropic composite thin-walled beams of closed cross-section contour. Journal of Sound and Vibration 167, 129–147.

Venkatesan, C., Friedmann, P.P., 1986. New approach to finite-state modeling of unsteady aerodynamics. AIAA Journal 24, 1889–1897.

Volovoi, V.V., Hodges, D.H., Cesnik, C.E.S., Popescu, B., 1999. Assessment of beam modeling methods for rotor blade applications. In: Journal of the American Helicopter Society, 55th Annual Forum, Montreal, Quebec, Canada, May 25–27.

von Kármán, T., Sears, W.R., 1938. Airfoil theory for non-uniform motion. Journal of the Aeronautical Sciences 5, 379–390.

Weisshaar, T.A., 1980. Forward swept wing static aeroelasticity, Final Report AFWAL-TR-80-3137.

Yates Jr., E.C., 1958. Calculation of flutter characteristics for finite-span swept or unswept wings at subsonic and supersonic speeds by a modified strip analysis. RM L57L10, NACA.